Check for updates

Insights into the differential fragmentation processes in rock avalanche emplacement from field investigation and experimental study

Yu-Feng Wang[1,2]*, Qian-Gong Cheng[1,2,3], Qi-Wen Lin[1], Kun Li[1] and Yan-Dong Ji[1]

[1]Department of Geological Engineering, Southwest Jiaotong University, Chengdu, Sichuan, China,
[2]Key Laboratory of High-Speed Railway Engineering, Ministry of Education, Chengdu, Sichuan, China,
[3]State-Province Joint Engineering Laboratory of Spatial Information Technology of High-Speed Rail
Safety, Chengdu, Sichuan, China

Fragmentation is a universal phenomenon associated with rock avalanches, resulting in an abundance of complex sedimentological structures. If studied in detail, these structures can provide insights into rock avalanche emplacement processes. Here, six typical avalanche cases are carefully analyzed in conjunction with an analogue experiment. Findings reveal the carapace facies is characterized by clast-supported structures composed of large blocks with sedimentological structures that include retained stratigraphic sequences, imbricate structures, and jigsaw structures. The body facies presents a high degree of fragmentation, with block-rich zones, fine matrix-rich zones, jigsaw structures, and inner shear zones. The basal facies displays the highest degree of fragmentation, however, it is mainly composed of millimeter grains with thin shear strips. Consistent with the field investigations, differential fragmentation is also observed in the analogue tests, with the vertical dimension of the carapace facies mainly fragmented along the lines of pre-existing structures; the body facies fragmented with an abundance of new fractures; and the basal facies fragmented into fine grains. Meanwhile, layer sequences preserved in longitudinal and vertical profiles are also observed in the analogue tests, indicating a low disturbance in the propagation. We, therefore, propose that a process characterized by a sparse state, dominated by collisions, minor disturbance, and pervasive dynamic fragmentation likely occurs in the carapace facies, with fragmentation mainly controlled by the breakage of pre-existing, fully-persistent structures. The body facies is mainly controlled by the fracturing of the weak, less-persistent structures, and the basal facies displays the highest degree of fragmentation with an abundance of new fractures. In the entire propagation, the avalanche mass displays low-disturbance laminar flow.

Introduction

The occurrence of rock avalanches has increased significantly in recent years and with sometimes catastrophic results, due to large volumes (>1×10^6 m³), extremely high velocities (>20 m/s), and long runouts (>1 km) (Evans et al., 2007; Sun et al., 2011; Huang et al., 2012; Pudasaini and Miller, 2013; Lucas et al., 2014; Iverson et al., 2015; Zhu et al., 2019; Friele et al., 2020; Zhang et al., 2020; Zhao et al., 2020). A typical example of such a disaster is the Xinmocun rock avalanche that occurred in China on June 24, 2017 (Fan et al., 2017). The detached mass transformed into a highly fragmented debris avalanche with a volume of 4.5×10^6 m³, which traveled downwards rapidly with a runout of up to 4.1 km within 110 s, burying the whole of Xinmocun downstream and killing about 100 people. It was calculated that the maximum velocity of the detached mass was over 50 m/s, thus presenting extremely high mobility (Fan et al., 2017). To explain the hypermobility of rock avalanches, some hypotheses have been proposed, including the frictional heating mechanism (Habib, 1975; He et al., 2015; Wang et al., 2017; Hu et al., 2019), dynamic fragmentation (Davies et al., 1999; Davies and McSaveney, 2009), substrate entrainment (Hungr and Evans, 2004; Iverson and Ouyang, 2015; Aaron and McDougall, 2019; Pudasaini and Krautblatter, 2021), shear induced fluidization (Melosh, 1979; Davies, 1982; Wang et al., 2015), and momentum transfer (Heim, 1932; Van Gassen and Cruden, 1989). Moreover, many studies focusing on field investigations (Hewitt et al., 2008; Weidinger et al., 2014; Dufresne et al., 2016a; Strom and Abdrakhmatov, 2018; Wang et al., 2018, 2019; Dufresne and Geertsema, 2020), laboratory experiments (Iverson et al., 2004; Shea and Vries, 2008; Manzella and Labiouse, 2009; Zhang and McSaveney, 2017; Li et al., 2021, 2022), and numerical simulations (Pudasaini and Hutter, 2007; Cagnoli and Piersanti, 2015; Mergili et al., 2018) have also been conducted to enable better understanding of the emplacement of rock avalanches.

Pervasive fragmentation in rock avalanches, as revealed by their deposits, has been commonly reported and is attracting increasing scientific attention (Hewitt, 2002; Locat et al., 2006; Crosta et al., 2007; Zhang et al., 2016; Dufresne and Dunning, 2017; Zhao et al., 2017; Ghaffari et al., 2019; Knapp and Krautblatter, 2020; Lin et al., 2020, 2021). With the occurrence of dynamic fragmentation in emplacement, crude inverse grading is a diagnostic feature in avalanche deposits, with three facies divided from bottom to top: basal facies, body facies, and carapace facies (Cruden and Hungr, 1986; Blair, 1999; Dunning, 2006; Dufresne et al., 2016b; Wang et al., 2018, 2019, 2020). In each facies, certain unique characteristics are well developed and widely distributed (Dufresne et al., 2016b). The basal facies is mainly composed of angular fine particles less than a centimeter in diameter with common entrainment of the substrate. In this facies, some minor internal sedimentological structures have been reported, such as diapiric structures, small-scale faults, and thin shear strips (Dufresne et al., 2016b; Wang

et al., 2019). The body facies mainly consists of highly-fragmented angular clasts, ranging in diameter from micrometer to decimeter scale. This facies is the main part of an avalanche deposit and is usually characterized by more internal sedimentological structures, such as block-rich zones, jigsaw structures, and inner shear zones. Because of the distribution of these structures in the vertical dimension, the body facies can be further divided into subfacies (Pollet and Schneider, 2004; Dufresne et al., 2016b). The carapace facies is the coarsest zone, with an abundance of angular blocks, characterized by a clast-supported structure with preserved source stratigraphy and jigsaw structures (Wang et al., 2019, 2020).

A better understanding of the fragmentation processes of these facies provides knowledge of the emplacement of rock avalanches and facilitates the evaluation of potential hazards. Focusing on the three facies outlined above, various studies have reported differential fragmentation (Davies et al., 1999; Strom, 1999; Pollet and Schneider, 2004; Dufresne et al., 2016b; Dufresne and Dunning, 2017; Strom and Abdrakhmatov, 2018). Furthermore, shear-related dynamical fluidization mechanisms have been proposed to explain the hypermobility of rock avalanches (Melosh, 1979; Davies, 1982; Davies and McSaveney, 2009; De Blasio and Crosta, 2015; Wang et al., 2015; Haug et al., 2016). However, studies focused on the differential fragmentation found in avalanche deposits remain limited and further work is needed to understand rock avalanche emplacement. To address this need, first, the surficial and internally deposited features of several typical cases were investigated in detail. An analogue study was then designed and conducted to reproduce the differential fragmentation processes of avalanche masses. Finally, a comparison of the field investigations and the analogue study was carried out, to understand the emplacement processes of rock avalanches from the viewpoint of differential fragmentation. A further aim is to provide sufficient field evidence and analogue data for use in future analogue and numerical studies of rock avalanches.

Regional geological setting

The study focuses on the Tibetan plateau, which formed ~55 Ma and resulted from the intensive and ongoing plate collision of India with Eurasia (Larson et al., 1999). The Tibetan plateau is the youngest and highest mountainous region in the world, characterized by a wide variety of geologies, geomorphologies, and climates. Global positioning system (GPS) data indicate that convergence is still occurring in the plateau, with numerous earthquakes generated (Larson et al., 1999; Tapponnier et al., 2001; Zhang et al., 2004). In just the past 100 years, there have been 36 events with $Ms > 7$, as reported by the Advanced National Seismic System (Figure 1).
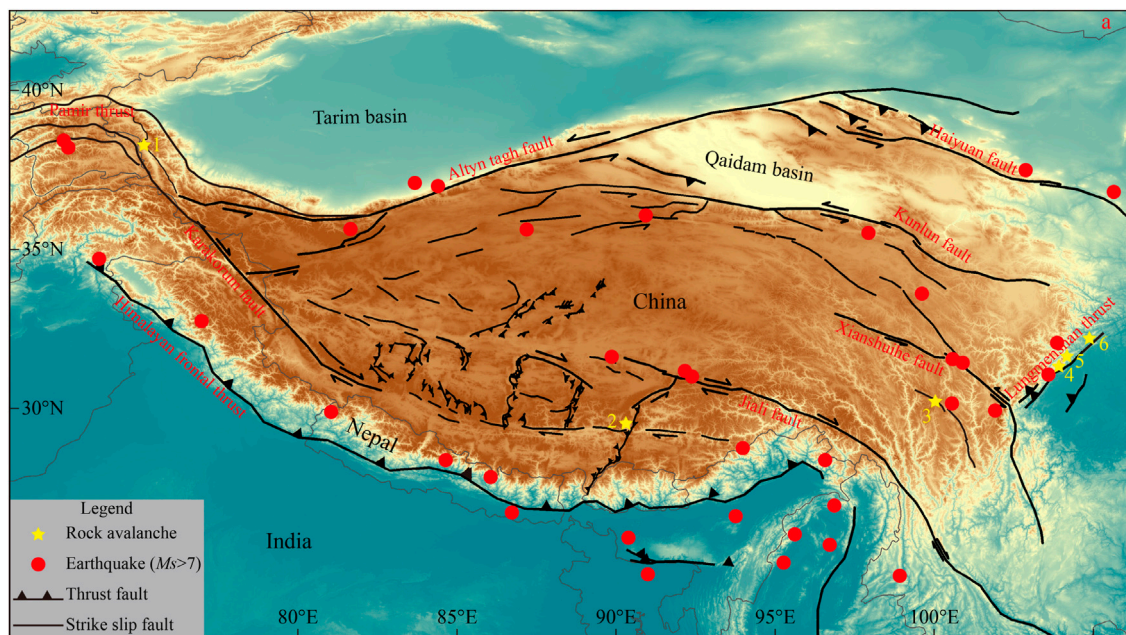
FIGURE 1
Geological map of the Tibetan plateau with the locations of the studied rock avalanches marked.

TABLE 1 Details of the studied rock avalanches.

No.	Name	Main lithology	Volume	Runout	Drop height	Fahrböschung	References
1	Tagarma rock avalanche	Gneiss	$\sim96 \times 10^6$ m^3	5.4 km	1,500 m	0.28	Wang et al. (2020)
2	Nyixoi Chongco rock avalanche	Biotite monzonitic granite	$\sim28 \times 10^6$ m^3	4.6 km	885 m	0.19	Wang et al. (2019)
3	Luanshibao rock avalanche	Biotite granodiorite	$\sim28 \times 10^6$ m^3	4.1 km	820 m	0.2	Wang et al. (2018)
4	Xiejiadianzi rock avalanche	Granite and granodiorite	$\sim3.5 \times 10^6$ m^3	1.7 km	700 m	0.41	Wang et al. (2015)
5	Daguangbao rock avalanche	Carbonate rocks and siltstone	$\sim7.5 \times 10^8$ m^3	4.3 km	1,300 m	0.30	Huang et al. (2012)
6	Donghekou rock avalanche	Slate and carbonate rocks	$\sim10 \times 10^6$ m^3	2.0 km	500 m	0.25	Sun et al. (2011)

Owing to the effects of intense tectonic activity and long-term weathering, intensely fractured bedrock is widely distributed with high topographic relief, which is thought to be particularly favorable for the generation of catastrophic bedrock landslides (Strom and Abdrakhmatov, 2018; Wang et al., 2018, 2019, 2020). Many massive rock avalanches have been reported in this area, and are increasingly attracting scientific attention (Yuan et al., 2013; Weidinger et al., 2014; Reznichenko et al., 2017; Strom and Abdrakhmatov, 2018; Wang et al., 2018, 2019, 2020). Figure 1 shows the locations of the rock avalanches investigated in this study, with three located along the Longmenshan thrust in the southeastern margin of the Tibetan plateau, and triggered by the Wenchuan earthquake in 2008. The remaining are prehistoric cases, with the Luanshibao rock avalanche in the Maoyaba basin along the Litang-Dewu fault

system, the Nyixoi Chongco rock avalanche in the Yadong-Gulu rift in the South Tibetan normal fault system, and the Tagarma rock avalanche in the Tarim basin of the Pamir-western Himalayan syntaxis. Table 1 lists some details of these cases. In Table 1, the Fahrböschung is defined as the ratio of the drop height (H) to the horizontal runout (L) between the crown and top, as proposed by Heim (1932) to quantify the hypermobility of rock avalanches.

Figure 2 shows the plan views of the studied rock avalanches, exhibiting the stereographic projections of the preferred structures developed in their source areas. As revealed in Figure 2, most of the cases studied are crossed by faults at the toes of their source areas, except for the Daguangbao and Donghekou rock avalanches, with faults nearly parallel to their flanks. Longitudinally, the topographies of their source
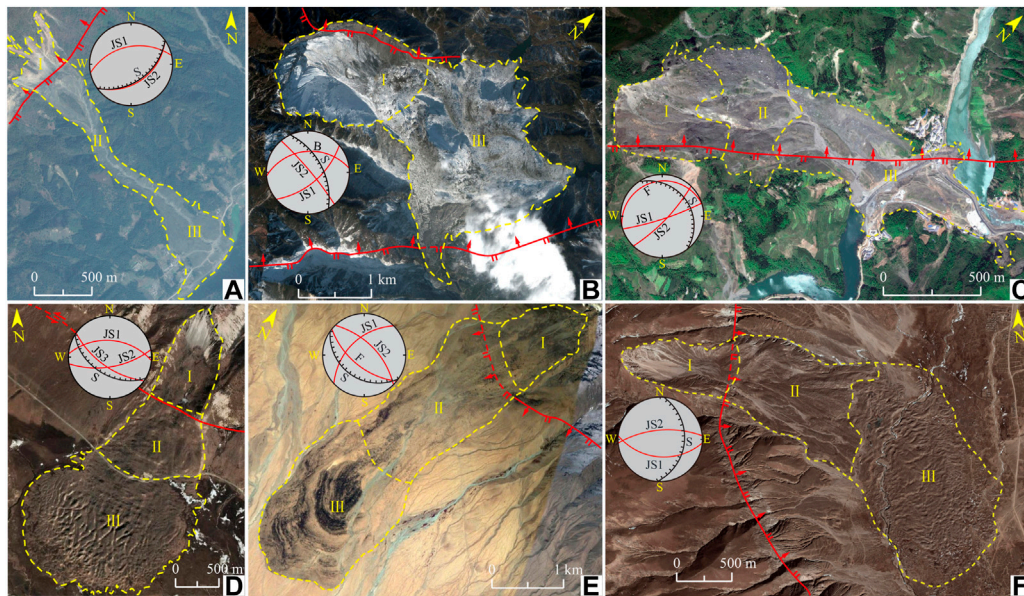
FIGURE 2
Remote images of the Xiejiadianzi **(A)**, Daguangbao **(B)**, Donghekou **(C)**, Luanshibao **(D)**, Tagarma **(E)**, and Nyixoi Chongco **(F)** rock avalanches with the stereographic projections of their source area preferred structures. JS, joints; F, foliation; S, slope; B, bedding plane; I: source area; II: transition zone; III: accumulation zone.

areas are steeper than their transition and accumulation zones. The lithologies of the source areas are different, with one originating in sedimentary rock, three originating in igneous rock, one originating in metamorphic rock, and one originating in mixed layers of sedimentary and metamorphic rock (Table 1). Highly fractured preferred structures are widely developed in their source areas (Figure 2), controlling failures of the bedrock. Unlike the source areas, the transition and accumulation zones are characterized by relatively planar topographies, with their substrates mainly consisting of quaternary deposits, including glacial moraine deposits, alluvial deposits, pluvial deposits, residual deposits, and talus.

Methods

Field investigation

Field investigations are the main method for examining the deposited characteristics of these rock avalanches, and these were performed based on Google Earth images, 1:200,000-scale geological maps, and 1:100,000-scale geomorphological maps. During the field investigations, high resolution cameras were employed to record these surficial and internal sedimentary structures, with a handheld Magellan global positioning system, a TruPulse200X laser rangefinder, and a compass used to confirm location, orientation, and size. 1:1,000-scale aerial images of the Nyixoi Chongco and Tagarma rock avalanches were acquired using fixed-wing unmanned aerial vehicles. The resolution of the aerial images is high enough to observe the surficial landforms of the avalanche carapace facies. Additionally, an area-by-area technique and sieve analyses were used to quantify the inverse grading features revealed by their internal vertical profiles.

Experimental setup

To explore the differential fragmentation in rock avalanche propagation, analogue model tests were also designed and conducted, with an overview of the experimental system given in Figure 3A. The experimental apparatus consists of an inclined flume (2.0 m long and 0.1 m wide), with its dip angle being 45°, a horizontal flume (2.4 m long and 0.1 m wide), and a material releasing box (0.4 m long and 0.1 m wide). Both of the side walls of the flumes are made of 0.8 cm thick plexiglass. To control the release of the material, a releasing gate was installed, as shown in Figure 3B.

To simulate the fragmentation process of avalanche masses in small-scale experiments, fragmentable analog material with relatively low strength was prepared using the scaling law based on the material properties of the Xiejiadianzi and Luanshibao rock avalanches. The main parameters used for the design of the analog material are σ (stress), E (elastic modulus), ϵ (strain), C
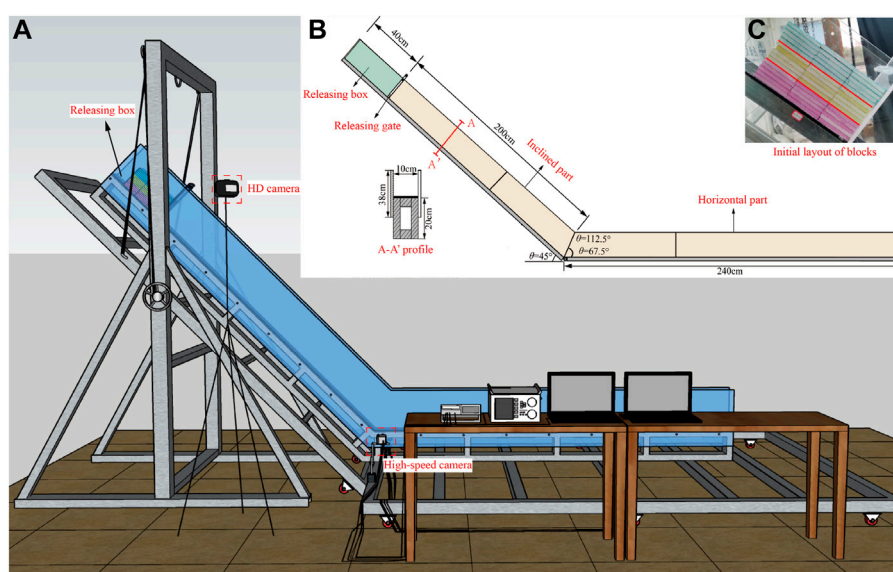
FIGURE 3
Schema of the experimental setup **(A,B)** and initial layout of blocks **(C)**.

TABLE 2 Parameters used for similarity analysis of the protype and similar materials.

	Bulk density/g/cm^3	Internal friction angle/°	Cohesion/MPa	Compressive strength/MPa	Elastic modulus/GPa
Symbol	ρ	φ	C	σ	E
Dimension	ML^{-3}	$M^0L^0T^0$	$ML^{-1}T^{-2}$	$ML^{-1}T^{-2}$	$ML^{-1}T^{-2}$
Scale ratio	1:1	1:1	1:600	1:600	1:600
Protype material	2.4–3.1	45–60	30–50	100–379	50–100
Similar materials	2.4–3.1	45–60	0.05–0.08	0.17–3.5	0.08–0.17

(cohesion), ϕ (internal friction angle), L (dimension), ρ (density), and g (gravitational acceleration), with the scaling law being as follows:

$$f\left(\sigma, E, \epsilon, C, \phi\right) = f\left(l, \rho, g\right) \qquad (1)$$

Referring to Lin et al. (2020), the scaling ratios of length, gravity, and material solid density were selected as the base dimensions, with their values being 600:1, 1:1, and 1:1, respectively. The values of the parameters used for the preparation of analogue material are listed in Table 2, and are according to dimensional analysis (Bolster et al., 2011; Iverson, 2015). Using the calculated values listed in Table 2, raw materials, including barite, quartz, gypsum, sodium silicate, sodium carboxymethyl cellulose, and glycerol were chosen to produce the fragmentable analog blocks, following the preparation process in Lin et al. (2020). The size of the analogue blocks was 100 * 100 *10 mm^3, with the compressive strength, elastic

modulus, cohesion, internal friction angle, and bulk density being 0.42 MPa, 106.56 MPa, 48.05 kPa, 29.39°, and 1.83 g cm^{-3}, respectively. The total weight of each test was 7.8 kg. To ensure the reproducibility of each test, three repeat tests were conducted.

For data collection, a high-speed camera (850 f/s) with 0.3 megapixels was used to record the fragmentation and propagation processes of the detached mass when it slid onto the horizontal plane, as shown in Figure 3. A 1080 p high-definition camera (HD camera), was employed to record the initial releasing process to make sure the release steps of each test were consistent. After the deposition of the detached mass in each test, the oblique photography technique was employed to obtain the final deposited characteristics (Li et al., 2021). The grain size distribution of each fragmented detached mass was calculated to quantify the degree of fragmentation.
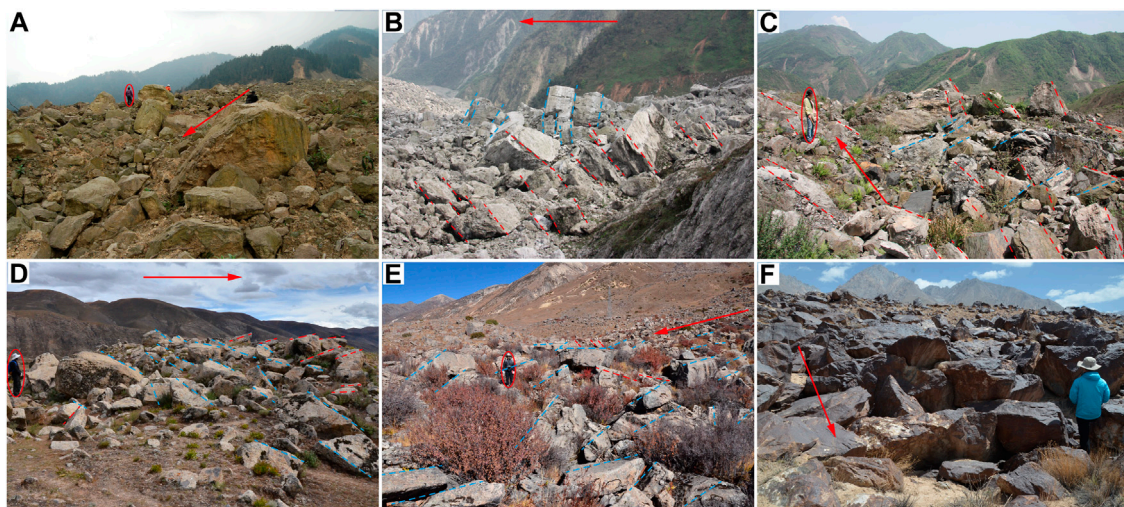
FIGURE 4
Clast-supported structures composed of blocks in the carapace facies of the Xiejiadianzi **(A)**, Daguangbao **(B)**, Donghekou **(C)**, Nyixoi Chongco **(D)**, Luanshibao **(E)**, and Tagarma **(F)** rock avalanches. The red arrow in each subfigure indicates the main movement direction of the avalanche masses with these dashed lines marking the preferred inclinations of fragmented blocks.

Depositional characteristics

The detached rock masses of the studied rock avalanches are characterized by variable volumes ($3.5–750 \times 10^6$ m³), runouts (2.0–5.4 km), and drop heights (500–1,500 m). It is calculated that their Fahrböschung values fall into the range of 0.19–0.41 (Table 1), indicating the high mobility of the mass propagations. Series of variable surficial characteristics were observed along their traveling paths, including ridges in varying shapes, scales, and orientations, toreva blocks, hummocks, jigsaw structures, and preserved bedrock sequences (Sun et al., 2011; Huang et al., 2012; Wang et al., 2012, 2018, 2019, 2020). Vertically, inverse grading was revealed, with three facies presented from bottom to top, i.e., basal facies, body facies, and carapace facies. In each facies, different sedimentary features were revealed. In the following, detailed descriptions of the depositional characteristics of the investigated cases are presented.

Depositional characteristics of the carapace facies

The carapace facies are characterized by wide distributions in particle size, ranging from micrometers to tens of meters, and mainly composed of blocks with clast-supported structures (Figure 4). Most blocks are irregular and angular, with very sharp edges, retaining their original fractured shapes. Controlled by internal structures, in most of the investigated rock avalanches blocks are mainly present in

tabular shapes of varying thickness. Their top and bottom surfaces are usually planar and smooth, especially in the Daguangbao, Donghekou, and Tagarma rock avalanches, with well-developed bedding or foliated structures.

As shown in Figures 4B–F, 5A, imbricate structures consisting of platy-shaped blocks (i.e., clusters of superimposed blocks fragmented to different extents) are commonly distributed, especially in the Daguangbao and Tagarma rock avalanches. The top surfaces of some imbricate structures face upstream (i.e., blocks marked by red dashed lines in Figures 4B–E) with the rest facing downstream (i.e., blocks marked by red dashed lines in Figures 4B–E). Figure 5A is an enlarged view showing the imbricate structures in the Tagarma rock avalanche with the top surface facing downstream. As exhibited in Figure 5A, the surface of each block is smooth and planar, indicating the control of foliation. Additionally, jigsaw structures are observed in the carapace facies, especially in the Daguangbao, Nyixoi Chongco, and Tagarma rock avalanches. Figure 5B shows one jigsaw structure observed in the Tagarma rock avalanche, with fragmented sub-blocks also presenting an imbricate structure, which is consistent with the structures of the source scar (Wang et al., 2020). Figures 5C–E show some jigsaw structures deposited in the Daguangbao rock avalanche, which are characterized by varying degrees of fragmentation. In the jigsaw structures shown in Figures 5C,D, original lithological sequences are well preserved with minor disturbance after fragmentation, indicating an extremely low disturbance in the propagation. Figure 5F shows one jigsaw structure observed in the Nyixoi Chongco rock avalanche.
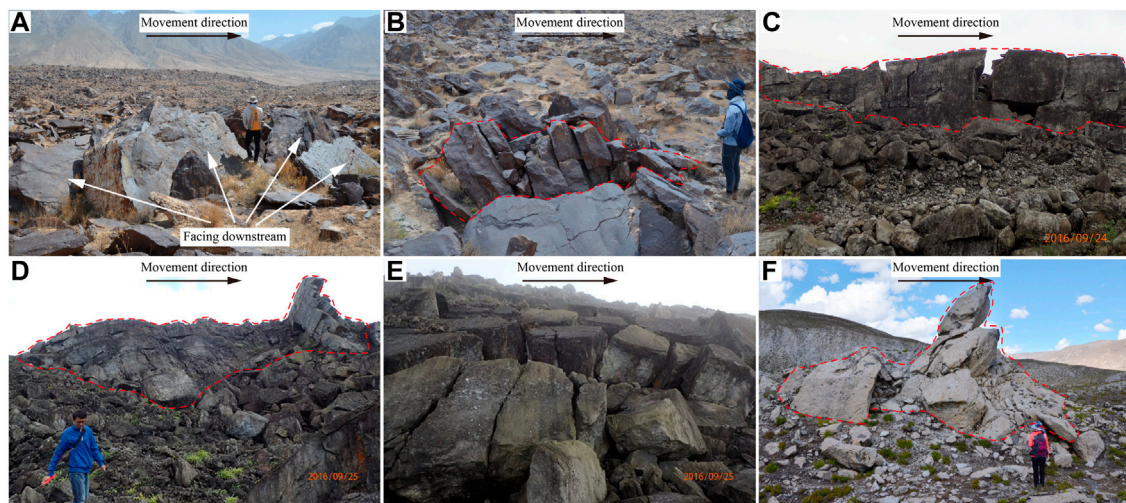
FIGURE 5
Photos showing imbricate structures **(A)** and jigsaw structures **(B–F)** deposited in the carapace facies of the Tagarma **(A,B)**, Daguangbao **(C–E)**, and Nyixoi Chongco **(F)** rock avalanches.
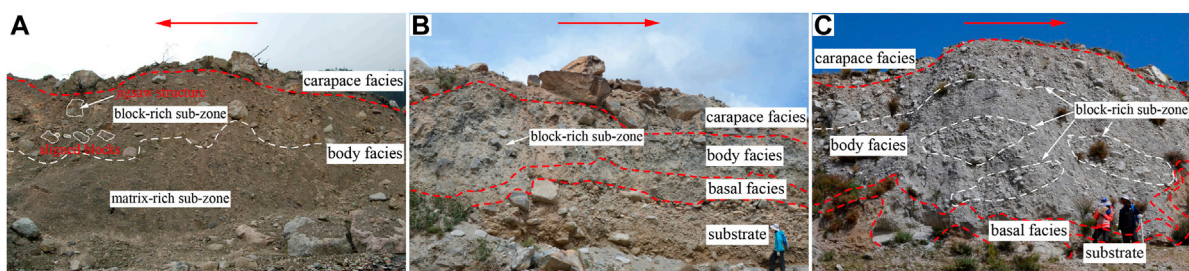
FIGURE 6
Deposited profiles of the Xiejiadianzi **(A)**, Tagarma **(B)**, and Nyixoi Chongco **(C)** rock avalanches. Red arrows indicate the movement directions of the avalanche mass.

Depositional characteristics of the body facies

Due to post-avalanche erosion, some well-preserved outcrops are revealed in the studied cases, providing opportunities to observe their internal sedimentary structures. As the outcrops reveal, the thicknesses of the body facies vary greatly versus runout under the control of underlying topographies, especially for the Nyixoi Chongco rock avalanche (Wang et al., 2012, 2019, 2020; Zeng et al., 2019). Figure 6 shows the deposited profiles of the Xiejiadianzi, Tagarma, and Nyixoi Chongco rock avalanches photographed during field surveys. The body facies are mainly composed of highly fragmented, angular clasts, ranging from micrometer to decimeter scales in diameter, which are obviously finer than those of the carapace facies. As the main part of rock avalanches, a series of internal sedimentological structures are observed, such as fine matrix-rich sub-zones, block-rich sub-zones, jigsaw structures, and inner shear bands (Wang et al., 2018, 2019, 2020).

As shown in Figure 6A, the body facies of the Xiejiadianzi rock avalanche can be further divided into a block-rich sub-zone with directionally aligned blocks and jigsaw structures, and a matrix-rich sub-zone mainly composed of micrometer to centimeter grains. In the outcrops of the Tagarma and Nyixoi Chongco rock avalanches, block-rich sub-zones are also observed, with directionally aligned clasts distributed as shown in Figures 6B,C. Grain sizes in the block-rich sub-zones mainly range in the dozens of decimeters along long axes.
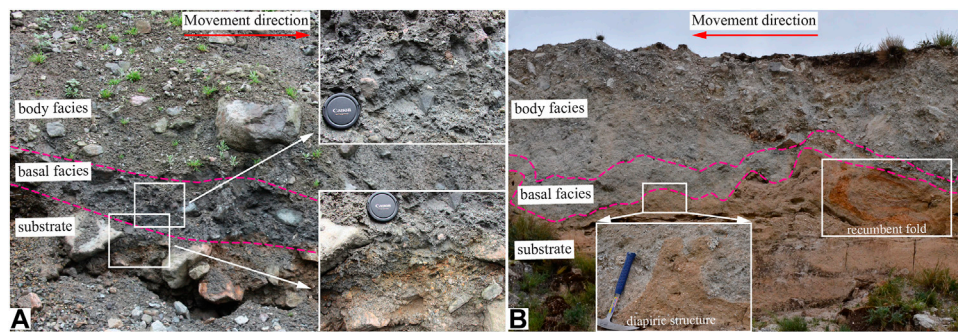
FIGURE 7
Layouts of the basal facies of the Xiejiadianzi **(A)** and Nyixoi Chongco **(B)** rock avalanches.

Depositional characteristics of the basal facies

The basal facies is the lowest zone of rock avalanches in direct contact with the substrate, and is the thinnest zone compared with the upper facies. It is usually less than 1 m in thickness. Due to the intensive interaction between the avalanche mass and the substrate, the fragmentation degree of this facies is obviously higher than the upper avalanche mass, with grains mainly finer than a centimeter in the long axes (Wang et al., 2012, 2015, 2019, 2020). Coarse clasts larger than several centimeters can also be observed occasionally. Figure 7 shows the layout of both outcrops of the Xiejiadianzi and Nyixoi Chongco rock avalanches. As shown in Figure 7A, grains in this facies also have angular shapes with low roundness, and are obviously different from the underlying rounded alluvial deposits. Additionally, intensively deformed shear structures can be observed in this facies and substrate (Figure 7B), including diapiric structures, convoluted laminations, faults, and basal décollements.

Experimental results

Figures 8A–F show the propagated process of the detached mass, with snapshots during 0.35–0.48 s presented in Figures 8G–J to reveal some detailed information about the propagation. From Figures 8A–F, it can be seen that the detached mass mainly behaves as a laminar flow during the whole propagation process with differential fragmentation in the vertical dimension. The snapshots shown in Figures 8G,H further prove the low disturbance of the detached mass in propagation, as the lines marked in red and yellow highlight the lamina flow. As the blocks circled by the red lines indicate, the ones on the top surface display a low fragmentation degree with its initial sequence preserved. The block marked by the

yellow lines is fragmented into small clasts, but still preserves its relationship with the upper blocks. Finally, a stratified internal structure, as observed in the source area, is generated in the final deposit (Figure 9A). Such a propagated model was already proposed by Strom in 2006. As exhibited in Figure 9A, a "multilayered" deposit is finally generated, due to pervasive fragmentation of differing extents during propagation, and similar to the inverse grading observed in rock avalanche deposits. According to the propagated features and final deposited sequence, the detached mass can be divided into three zones from rear to front, i.e., the tensional zone, compressional zone, and spreading zone (Figure 9A), which is consistent with the propagated processes proposed in some rock avalanches (Wang et al., 2018, 2019). The frontal spreading zone is relatively thin with clasts deposited relatively sparsely. The deposit in the middle compressional zone is thickest, with some compressed features present, such as folds. Furthermore, some deposited structures, including clast-supported (Figure 9A) and jigsaw structures (Figures 9B,C), can be observed.

To give a more direct sense of the vertical differential fragmentation of the detached mass, the deposited mass was divided into three layers from top to bottom, i.e., the upper, middle, and lower layers, as shown in Figures 9B–D. It can be seen that the upper layer is mainly composed of non-fragmented and low-fragmented blocks. In the propagation, they were mainly fragmented along the pre-existing, fully persistent discontinuities among blocks. Imbricate structures and retained original stratigraphic structures, similar to those observed in the Tagarma and Daguangbao rock avalanches, are widely distributed in the upper layer. The fragmentation degree of the middle layer increases obviously, with most blocks fragmented into clasts of centimeter size. Although the fragmentation degree increases, jigsaw structures are commonly developed in this layer, which is similar to that observed in the
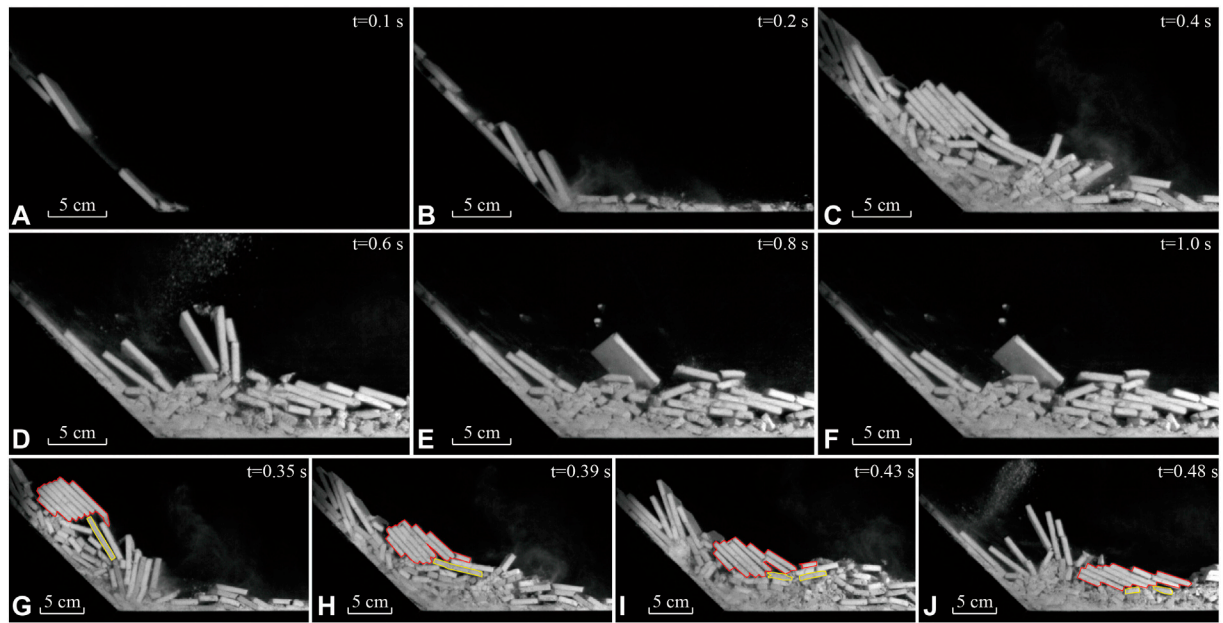
FIGURE 8
Photos recording the propagated process of the detached mass **(A–F)** with snapshots during t = 0.35−0.48 s. The red and yellow lines in **G–J** mark the distribution of preserved block sequence.
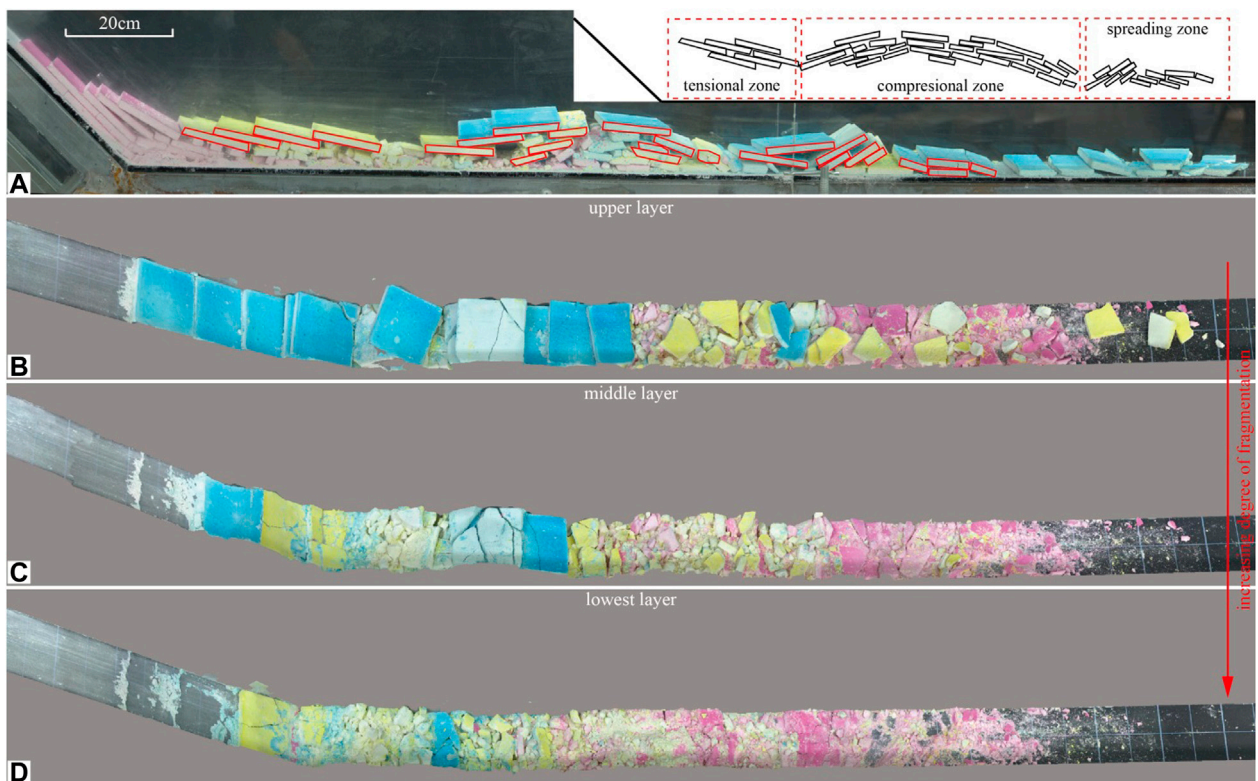
FIGURE 9
Final deposit of the detached mass **(A)** with vertical layering of the deposit from top to bottom **(B–D)**.

avalanche cases. The lowest layer is completely composed of fragmented blocks, with the most fragmented in millimeter size.

Discussion

As described above, the deposit of the experimental study presents an inverse grading feature with a clast-supported structure, retained original stratigraphic structure, imbricate structure, jigsaw structure, and folds, which is similar to that observed in natural rock avalanches. As argued by Strom (1994, 1999), retained original stratigraphic structures are commonly distributed in rock avalanches that occurred in the Pamir and Tian-Shan Mountains and are suggested as indicators of a slight disturbance in avalanche propagation (Strom, 1994, 1999). Jigsaw structures commonly observed in rock avalanches have also been regarded as indicators of a slight internal disturbance in the propagation of an avalanche mass (Paguican et al., 2014; Dufresne et al., 2016b; Wang et al., 2019). Hence, we believe the high consistency between the experimental results and the field observations further proves that a relatively steady movement, with differential fragmentation and slight internal disturbance, should be considered the main propagation form of rock avalanches.

During the propagation, the detached mass in the carapace facies is in a relatively sparse state, with clasts mainly suffering a relatively low stress level dominated by collisions. Fragmentation in the carapace facies is mainly controlled by the breakage of pre-existing fully persistent discontinuities with low stress levels that already existed in the bedrock when detaching from the source area (Charrière et al., 2016; Wang et al., 2020). Furthermore, fragmentation associated with breakages of rock bridges of less persistent structures also occurs, due to continued dynamic interactions among blocks. The body and basal facies are in a relatively dense state with intensive fragmentation occurring. Fragmentation in the body and basal facies is associated with the breakages of rock bridges of less-persistent structures or the generation of new fractures. The stress level suffered by the body and basal facies is higher than that of the carapace facies.

Conclusion

To understand the differential fragmentation and propagation mechanisms of rock avalanches, the sedimentological features of several natural cases were investigated here in detail along their entire travel paths. Furthermore, an analogue model study was conducted to verify the ideas based on the field investigated data. The main findings are as follows:

1) The carapace facies is a commonly observed sedimentological unit in rock avalanche deposits, featuring large blocks armoring the depositional surface. Clasts in this facies are deposited in a relatively sparse state, with a series of complex sedimentological structures, including conservation of stratigraphic sequences, clast-supported structures, imbricate structures, and jigsaw structures. Compared with the carapace facies, the body and basal facies display in a dense state with higher fragmentation.

2) The analogue model results reveal that the detached mass mainly behaves as a laminar flow during propagation with stratified internal structures, as observed in the source area generated in the final deposit. In the propagation, pervasive fragmentation of differing extents occurs in the vertical dimension, with the formation of a "multilayered" deposit. The mass near the top surface is in a sparse state during propagation, and is mainly dominated by impact collisions with the lower main body, and presenting a dense flow.

3) Based on the high consistency of the sedimentological structures obtained from the field investigations and analogue model, we propose that rock avalanches should display in a laminar-dominated propagation with vertical differential fragmentation. The carapace facies should propagate in a sparse state, dominated by impact collisions. During propagation, the facies is characterized by minor disturbance and pervasive dynamic fragmentation. The dynamic fragmentation process is mainly controlled by the breakage of pre-existing, fully persistent structures with low stress levels. The body and basal facies should propagate in a dense state dominated by shearing. During intensive shearing, abundant new fractures are generated, resulting in a higher degree of fragmentation.

Through detailed field investigations and a primary analogue model study of the propagated and deposited features of rock avalanches, possible explanations of their propagation mechanisms are proposed in this study. With this study, we hope to provide more field evidence and laboratory data that can be used in further studies of rock avalanches.

Data availability statement

The original contributions presented in the study are included in the article/Supplementary Material, and further inquiries can be directed to the corresponding author.

Author contributions

Y-FW contributed to all the work related to the manuscript; Q-GC contributed to the field investigation and manuscript writing; Q-WL and KL contributed to the field investigation; and Y-DJ contributed to the experimental study.

Funding

Acknowledgments

Conflict of interest

The authors declare that the research was conducted in the absence of any commercial or financial relationships that could be construed as a potential conflict of interest.

Publisher's note

All claims expressed in this article are solely those of the authors and do not necessarily represent those of their affiliated organizations, or those of the publisher, the editors, and the reviewers. Any product that may be evaluated in this article, or claim that may be made by its manufacturer, is not guaranteed or endorsed by the publisher.

References

Aaron, J., and McDougall, S. (2019). Rock avalanche mobility: The role of path material. *Eng. Geol.* 257, 105126. doi:10.1016/j.enggeo.2019.05.003

Blair, T. C. (1999). Form, facies, and depositional history of the north long john rock avalanche, owens valley, California. *Can. J. Earth Sci.* 36 (6), 855–870. doi:10.1139/e99-024

Bolster, D., Hershberger, R. E., and Donnelly, R. J. (2011). Dynamic similarity, the dimensionless science. *Phys. Today* 64 (9), 42–47. doi:10.1063/pt.3.1258

Cagnoli, B., and Piersanti, A. (2015). Grain size and flow volume effects on granular flow mobility in numerical simulations: 3-D discrete element modeling of flows of angular rock fragments. *J. Geophys. Res. Solid Earth* 120 (4), 2350–2366. doi:10.1002/2014jb011729

Charrière, M., Humair, F., Froese, C., Jaboyedoff, M., Pedrazzini, A., and Longchamp, C. (2016). From the source area to the deposit: Collapse, fragmentation, and propagation of the frank slide. *GSA Bull.* 128 (1-2), 332–351. doi:10.1130/B31243.1

Crosta, G. B., Frattini, P., and Fuis, N. (2007). Fragmentation in the val pola rock avalanche, Italian alps. *J. Geophys. Res. Earth Surf.* 112 (F1). doi:10.1029/2005JF000455

Cruden, D. M., and Hungr, O. (1986). The debris of the Frank slide and theories of rockslide-avalanche mobility. *Can. J. Earth Sci.* 23 (3), 425–432. doi:10.1139/e86-044

Davies, T. R. H., McSaveney, M. J., and Hodgson, K. A. (1999). A fragmentation-spreading model for long-runout rock avalanches. *Can. Geotech. J.* 36 (6), 1096–1110. doi:10.1139/t99-067

Davies, T. R. H., and McSaveney, M. J. (2009). The role of rock fragmentation in the motion of large landslides. *Eng. Geol.* 109 (1-2), 67–79. doi:10.1016/j.enggeo.2008.11.004

Davies, T. R. H. (1982). Spreading of rock avalanche debris by mechanical fluidization. *Rock Mech.* 15 (1), 9–24. doi:10.1007/bf01239474

De Blasio, F. V., and Crosta, G. B. (2015). Fragmentation and boosting of rock falls and rock avalanches. *Geophys. Res. Lett.* 42, 8463–8470. doi:10.1002/2015gl064723

Dufresne, A., Bösmeier, A., and Prager, C. (2016b). Sedimentology of rock avalanche deposits – case study and review. *Earth. Sci. Rev.* 163, 234–259. doi:10.1016/j.earscirev.2016.10.002

Dufresne, A., and Dunning, S. A. (2017). Process dependence of grain size distributions in rock avalanche deposits. *Landslides* 14, 1555–1563. doi:10.1007/s10346-017-0806-y

Dufresne, A., and Geertsema, I. M. (2020). Rock slide-debris avalanches: Flow transformation and hummock formation, examples from British columbia. *Landslides* 17, 15–32. doi:10.1007/s10346-019-01280-x

Dufresne, A., Prager, C., and Bösmeier, A. (2016a). Insights into rock avalanche emplacement processes from detailed morpho-lithological studies of the Tschirgant deposit (Tyrol, Austria). *Earth Surf. Process. Landf.* 41 (5), 587–602. doi:10.1002/esp.3847

Dunning, S. A. (2006). The grain size distribution of rock-avalanche deposits in valley-confined settings. *Italian J. Eng. Geol. Environ.* 1(S1), 117–121. doi:10.4408/IJEGE.2006-01.S-15

Evans, S. G., Guthrie, R. H., Roberts, N. J., and Bishop, N. F. (2007). The disastrous 17 february 2006 rockslide-debris avalanche on leyte island, Philippines: A catastrophic landslide in tropical mountain terrain. *Nat. Hazards Earth Syst. Sci.* 7, 89–101. doi:10.5194/nhess-7-89-2007

Fan, X. M., Xu, Q., Scaringi, G., Dai, L. X., Li, W. L., Dong, X. J., et al. (2017). Failure mechanism and kinematics of the deadly June 24th 2017 xinmo landslide, maoxian, sichuan, China. *Landslides* 15, 2129–2146. doi:10.1007/s10346-017-0907-7

Friele, P., Millard, T. H., Mitchell, A., Allstadt, K. E., Menounos, B., Geertsema, M., et al. (2020). Observations on the may 2019 joffre peak landslides, British columbia. *Landslides* 17, 913–930. doi:10.1007/s10346-019-01332-2

Ghaffari, H., Griffith, W., and Barber, T. (2019). Energy delocalization during dynamic rock fragmentation. *Geophys. J. Int.* 217 (2), 1034–1046. doi:10.1093/gji/ggz064

Habib, P. (1975). Production of gaseous pore pressure during rock slides. *Rock Mech.* 7 (4), 193–197. doi:10.1007/bf01246865

Haug, Ø. T., Rosenau, M., Leever, K., and Oncken, O. (2016). On the energy budgets of fragmenting rockfalls and rockslides: Insights from experiments. *J. Geophys. Res. Earth Surf.* 121, 1310–1327. doi:10.1002/2014jf003406

He, S. M., Liu, W., and Wang, J. (2015). Dynamic simulation of landslide based on thermo-poro-elastic approach. *Comput. Geosciences* 75, 24–32. doi:10.1016/j.cageo.2014.10.013

Heim, A. (1932). *Landslides and human lives*. Vancouver: Bitech Publishers, 1–203.

Hewitt, K., Clague, J. J., and Orwin, J. F. (2008). Legacies of catastrophic rock slope failures in mountain landscapes. *Earth-Science Rev.* 87 (1-2), 1–38. doi:10.1016/j.earscirev.2007.10.002

Hewitt, K. (2002). Styles of rock avalanche depositional complexes conditioned by very rugged terrain, Karakoram Himalaya, Pakistan. *Rev. Eng. Geol.* 15, 345–377. doi:10.1130/reg15-p345

Hu, W., Huang, R. Q., McSaveney, M., Yao, L., Xu, Q., Feng, M. S., et al. (2019). Superheated steam, hot CO_2 and dynamic recrystallization from frictional heat jointly lubricated a giant landslide: Field and experimental evidence. *Earth Planet. Sci. Lett.* 510, 85–93. doi:10.1016/j.epsl.2019.01.005

Huang, R. Q., Pei, X. J., Fan, X. M., Zhang, W. F., Li, S. G., and Li, B. L. (2012). The characteristics and failure mechanism of the largest landslide triggered by the Wenchuan earthquake, May 12, 2008, China. *Landslides* 9 (1), 131–142. doi:10.1007/s10346-011-0276-6

Hungr, O., and Evans, S. G. (2004). Entrainment of debris in rock avalanches: An analysis of a long run-out mechanism. *Geol. Soc. Am. Bull.* 116 (9/10), 1240–1252. doi:10.1130/b25362.1

Iverson, R. M., George, D. L., Allstadt, K., Reid, M. E., Collins, B. D., Vallance, J. W., et al. (2015). Landslide mobility and hazards: Implications of the 2014 oso disaster. *Earth Planet. Sci. Lett.* 412, 197–208. doi:10.1016/j.epsl.2014.12.020

Iverson, R. M., Logan, M., and Denlinger, R. P. (2004). Granular avalanches across irregular three-dimensional terrain: 2. Experimental tests. *J. Geophys. Res.* 109 (F1). doi:10.1029/2003jf000084

Iverson, R. M., and Ouyang, C. J. (2015). Entrainment of bed material by Earth-surface mass flows: Review and reformulation of depth-integrated theory. *Rev. Geophys.* 53 (1), 27–58. doi:10.1002/2013rg000447

Iverson, R. M. (2015). Scaling and design of landslide and debris-flow experiments. *Geomorphology* 244 (SI), 9–20. doi:10.1016/j.geomorph.2015.02.033

Knapp, S., and Krautblatter, M. (2020). Conceptual framework of energy dissipation during disintegration in rock avalanches. *Front. Earth Sci. (Lausanne).* 8, 263. doi:10.3389/feart.2020.00263

Larson, K. M., Roland, B., Bilham, R., and Freymueller, J. T. (1999). Kinematics of the India-Eurasia collision zone from GPS measurements. *J. Geophys. Res.* 104 (B1), 1077–1093. doi:10.1029/1998jb900043

Li, K., Wang, Y. F., Cheng, Q. G., Lin, Q. W., Wu, Y., and Long, Y. M. (2022). Insight into granular flow dynamics relying on basal stress measurements: From experimental flume tests. *JGR. Solid Earth* 127 (3). doi:10.1029/2021jb022905

Li, K., Wang, Y. F., Lin, Q. W., Cheng, Q. G., and Wu, Y. (2021). Experiments on granular flow behavior and deposit characteristics: Implications for rock avalanche kinematics. *Landslides* 18 (5), 1779–1799. doi:10.1007/s10346-020-01607-z

Lin, Q. W., Cheng, Q. G., Li, K., Xie, Y., and Wang, Y. F. (2020). Contributions of rockmass structure to the emplacement of fragmenting rockfalls and rockslides: Insights from laboratory experiments. *J. Geophys. Res. Solid Earth* 125 (4). doi:10.1029/2019jb019296

Lin, Q. W., Cheng, Q. G., Xie, Y., Zhang, F. S., Li, K., Wang, Y. F., et al. (2021). Simulation of the fragmentation and propagation of jointed rock masses in rockslides: DEM modeling and physical experimental verification. *Landslides* 18 (3), 993–1009. doi:10.1007/s10346-020-01542-z

Locat, P., Couture, R., Locat, J., Leroueil, S., and Jaboyedoff, M. (2006). Fragmentation energy in rock avalanches. *Can. Geotech. J.* 43 (8), 830–851. doi:10.1139/t06-045

Lucas, A., Mangeney, A., and Ampuero, J. P. (2014). Frictional velocity-weakening in landslides on Earth and on other planetary bodies. *Nat. Commun.* 5 (9), 3417. doi:10.1038/ncomms4417

Manzella, I., and Labiouse, V. (2009). Flow experiments with gravel and blocks at small scale to investigate parameters and mechanisms involved in rock avalanches. *Eng. Geol.* 109 (1-2), 146–158. doi:10.1016/j.enggeo.2008.11.006

Melosh, H. J. (1979). Acoustic fluidization: A new geological process? *J. Geophys. Res.* 84 (B13), 7513–7520. doi:10.1029/jb084ib13p07513

Mergili, M., Frank, B., Fischer, J. T., Huggel, C., and Pudasaini, S. P. (2018). Computational experiments on the 1962 and 1970 landslide events at Huascarán (Peru) with r.avaflow: Lessons learned for predictive mass flow simulations. *Geomorphology* 322, 15–28. doi:10.1016/j.geomorph.2018.08.032

Paguican, E. M. R., van Wyk de Vries, B., and Lagmay, A. F. M. (2014). Hummocks: How they form and how they evolve in rockslide-debris avalanches. *Landslides* 11 (1), 67–80. doi:10.1007/s10346-012-0368-y

Pollet, N., and Schneider, J. L. M. (2004). Dynamic disintegration processes accompanying transport of the holocene flims sturzstrom (Swiss alps). *Earth Planet. Sci. Lett.* 221 (1-4), 433–448. doi:10.1016/s0012-821x(04)00071-8

Pudasaini, S. P., and Hutter, K. (2007). *Avalanche dynamics: Dynamics of rapid flows of dense granular avalanches.* Verlag Berlin Heidelberg: Springer, 1–602.

Pudasaini, S. P., and Krautblatter, M. (2021). The mechanics of landslide mobility with erosion. *Nat. Commun.* 12, 6793. doi:10.1038/s41467-021-26959-5

Pudasaini, S. P., and Miller, S. A. (2013). The hypermobility of huge landslides and avalanches. *Eng. Geol.* 157, 124–132. doi:10.1016/j.enggeo.2013.01.012

Reznichenko, N. V., Andrews, G. R., Geater, R. E., and Strom, A. (2017). Multiple origins of large hummock deposits in alai valley, northern Pamir: Implications for palaeoclimate reconstructions. *Geomorphology* 285, 347–362. doi:10.1016/j.geomorph.2017.02.019

Shea, T., and Vries, B. W. (2008). Structural analysis and analogue modeling of the kinematics and dynamics of rockslide avalanches. *Geosphere* 4 (4), 657–686. doi:10.1130/ges00131.1

Strom, A., and Abdrakhmatov, K. (2018). *Rockslides and rock avalanches of central asia.* Netherlands: Elsevier, 1–424.

Strom, A. 1994. Mechanism of stratification and abnormal crushing of rockslide deposits. In: Proceedings of the 7th International IAEG Congress 3. Balkema, Rotterdam, 9 September, 1994, pp. 1287–1295.

Strom, A. (1999). The morphology and internal structure of large rockslides as indicators of their formational mechanisms. *Dokl. Akad. Nauk.* 369 (1), 1079–1081.

Sun, P., Zhang, Y. S., Shi, J. S., and Chen, L. W. (2011). Analysis on the dynamical process of Donghekou rockslide-debris flow triggered by 5.12 Wenchuan earthquake. *J. Mt. Sci.* 8 (2), 140–148. doi:10.1007/s11629-011-2112-9

Tapponnier, P., Xu, Z. Q., Roger, F., Meyer, B., Arnaud, N., Wittlinger, G., et al. (2001). Oblique stepwise rise and growth of the Tibet plateau. *Science* 294 (5547), 1671–1677. doi:10.1126/science.105978

Van Gassen, W., and Cruden, D. M. (1989). Momentum transfer and friction in the debris of rock avalanches. *Can. Geotech. J.* 26 (4), 623–628. doi:10.1139/t89-075

Wang, Y. F., Cheng, Q. G., Lin, Q. W., Li, K., and Yang, H. F. (2018). Insights into the kinematics and dynamics of the Luanshibao rock avalanche (Tibetan Plateau, China) based on its complex surface landforms. *Geomorphology* 317, 170–183. doi:10.1016/j.geomorph.2018.05.025

Wang, Y. F., Cheng, Q. G., Shi, A. W., Yuan, Y. Q., Qiu, Y. H., and Yin, B. M. (2019). Characteristics and transport mechanism of the Nyixoi Chongco rock avalanche on the Tibetan Plateau, China. *Geomorphology* 343, 92–105. doi:10.1016/j.geomorph.2019.07.002

Wang, Y. F., Cheng, Q. G., Yuan, Y. Q., Wang, J., Qiu, Y. H., Yin, B. M., et al. (2020). Emplacement mechanisms of the Tagarma rock avalanche on the pamir-western himalayan syntaxis of the Tibetan plateau, China. *Landslides* 17, 527–542. doi:10.1007/s10346-019-01298-1

Wang, Y. F., Cheng, Q. G., and Zhu, Q. (2012). Inverse grading analysis of deposit from rock avalanches triggered by Wenchuan earthquake. *Chin. J. Rock Mech. Eng.* 31 (6), 1089–1106. in Chinese. doi:10.3969/j.issn.1000-6915.2012.06.002

Wang, Y. F., Cheng, Q. G., and Zhu, Q. (2015). Surface microscopic examination of quartz grains from rock avalanche basal facies. *Can. Geotech. J.* 52 (2), 167–181. doi:10.1139/cgj-2013-0284

Wang, Y. F., Dong, J. J., and Cheng, Q. G. (2017). Velocity-dependent frictional weakening of large rock avalanche basal facies: Implications for rock avalanche hypermobility? *J. Geophys. Res. Solid Earth* 122 (3), 1648–1676. doi:10.1002/2016jb013624

Weidinger, J. T., Korup, O., Munack, H., Altenberger, U., Dunning, S., Tipelt, G., et al. (2014). Giant rockslides from the inside. *Earth Planet. Sci. Lett.* 389, 62–73. doi:10.1016/j.epsl.2013.12.017

Yuan, Z. D., Chen, J., Owen, L. A., Hedrick, K. A., Caffee, M. W., Li, W. Q., et al. (2013). Nature and timing of large landslides within an active orogen, eastern Pamir, China. *Geomorphology* 182, 49–65. doi:10.1016/j.geomorph.2012.10.028

Zeng, Q. L., Zhang, L. Q., Davies, T., Yuan, G. X., Xue, X. Y., Wei, R. Q., et al. (2019). Morphology and inner structure of Luanshibao rock avalanche in Litang, China and its implications for long-runout mechanisms. *Eng. Geol.* 260, 105216. doi:10.1016/j.enggeo.2019.105216

Zhang, M., and McSaveney, M. (2017). Rock avalanche deposits store quantitative evidence on internal shear during runout. *Geophys. Res. Lett.* 44 (17), 8814–8821. doi:10.1002/2017gl073774

Zhang, M., Yin, Y. P., and McSaveney, M. (2016). Dynamics of the 2008 earthquake-triggered Wenjiagou creek rock avalanche, Qingping, Sichuan, China. *Eng. Geol.* 200, 75–87. doi:10.1016/j.enggeo.2015.12.008

Zhang, P. Z., Shen, Z., Wang, M., Gan, W. J., Bürgmann, R., Molnar, P., et al. (2004). Continuous deformation of the Tibetan Plateau from global positioning system data. *Geol.* 32 (9), 809–812. doi:10.1130/g20554.1

Zhang, Y. B., Xing, A. G., Jin, K. P., Zhuang, Y., Bilal, M., Xu, S. M., et al. (2020). Investigation and dynamic analyses of rockslide-induced debris avalanche in Shuicheng, Guizhou, China. *Landslides* 17, 2189–2203. doi:10.1007/s10346-020-01436-0

Zhao, T., Crosta, G. B., Utili, S., and De Blasio, F. V. (2017). Investigation of rock fragmentation during rockfalls and rock avalanches via 3-D discrete element analyses. *J. Geophys. Res. Earth Surf.* 122 (3), 678–695. doi:10.1002/2016jf004060

Zhao, W. H., Wang, R., Liu, X. W., Ju, N. P., and Xie, M. L. (2020). Field survey of a catastrophic high-speed long-runout landslide in jichang town, shuicheng county, guizhou, China, on july 23, 2019. *Landslides* 17 (6), 1415–1427. doi:10.1007/s10346-020-01380-z

Zhu, Y. Q., Xu, S. M., Zhuang, Y., Dai, X. J., Lv, G., and Xing, A. G. (2019). Characteristics and runout behaviour of the disastrous 28 August 2017 rock avalanche in Nayong, Guizhou, China. *Eng. Geol.* 259, 105154. doi:10.1016/j.enggeo.2019.105154